Thermodynamics of the $S = \frac{1}{2}$ hyperkagome-lattice Heisenberg antiferromagnet

Taras Hutak,[1] Taras Krokhmalskii,[1] Jürgen Schnack,[2] Johannes Richter,[3,4] and Oleg Derzhko[1,2,5,*]

[1]*Institute for Condensed Matter Physics, National Academy of Sciences of Ukraine, 79011 L'viv, Ukraine*

[2]*Fakultät für Physik, Universität Bielefeld, 33501 Bielefeld, Germany*

[3]*Institut für Physik, Otto-von-Guericke-Universität Magdeburg, 39016 Magdeburg, Germany*

[4]*Max-Planck-Institut für Physik komplexer Systeme, 01187 Dresden, Germany*

[5]*Professor Ivan Vakarchuk Department for Theoretical Physics, Ivan Franko National University of L'viv, 79005 L'viv, Ukraine*

(Received 14 November 2023; revised 9 July 2024; accepted 2 August 2024; published 15 August 2024)

The $S = 1/2$ hyperkagome-lattice Heisenberg antiferromagnet allows us to study the interplay of geometrical frustration and quantum as well as thermal fluctuations in three dimensions. We use 16 terms of a high-temperature series expansion complemented by the entropy-method interpolation to examine the specific heat and the uniform susceptibility of this model. We obtain thermodynamic quantities for several possible scenarios determined by the behavior of the specific heat as $T \to 0$: A power-law decay with the exponent $\alpha = 1$, 2, and also 3 (gapless energy spectrum) or an exponential decay (gapped energy spectrum). All scenarios give rise to a low-temperature peak in $c(T)$ (almost a shoulder for $\alpha = 1$) at $T < 0.05$, i.e., well below the main high-temperature peak. The functional form of the uniform susceptibility $\chi(T)$ below about $T = 0.5$ depends strongly not only on the chosen scenario but also on an input parameter $\chi_0 \equiv \chi(T = 0)$. An estimate for the ground-state energy e_0 depends on the adopted specific scenario but is expected to lie between -0.441 and -0.435. In addition to the entropy-method interpolation we use the finite-temperature Lanczos method to calculate $c(T)$ and $\chi(T)$ for finite lattices of $N = 24$ and 36 sites. A combined view on both methods leads us to favor the gapless scenario with $\alpha = 2$ (but $\alpha = 1$ cannot be excluded) and finite χ_0 around 0.1.

DOI: 10.1103/PhysRevB.110.054428

I. INTRODUCTION

Frustrated quantum spin systems are a subject of intense ongoing research in the field of magnetism [1–4]. Geometric frustration and quantum fluctuations may prevent any ground-state ordering even in three dimensions. Among several famous examples, the $S = 1/2$ pyrochlore-lattice Heisenberg antiferromagnet has attracted much attention, being for decades a candidate for the realization of a spin-liquid state in three dimensions [5]. After intense numerical studies, a lattice symmetry breaking in the ground state has been revealed [6–9].

A closely related example is the $S = 1/2$ hyperkagome-lattice Heisenberg antiferromagnet. Inspired by experiments on the spinel oxide $Na_4Ir_3O_8$ [10], in which low spin d^5 Ir^{4+} ions reside on the vertices of a hyperkagome lattice, several theoretical studies for the classical ($S \to \infty$) and quantum ($S = 1/2$) Heisenberg antiferromagnet on such a lattice have been performed [11–19]. The main focus of these studies is at ground-state properties of the $S = 1/2$ hyperkagome-lattice Heisenberg antiferromagnet. For the ground state of this model a gapped quantum spin liquid with topological order [12] and a gapless quantum spin liquid with spinon Fermi surfaces [15] were proposed by Lawler *et al.*. While the former proposal implies a nonzero spin gap, the latter one points to gapless spin excitations. In contrast, Bergholtz *et al.* [16] proposed a valence bond crystal with a 72-site unit cell as the ground state of this model (thus, breaking translational symmetry but not spin-rotational one). This proposal implies a spin gap with a huge number of singlet excitations below the lowest triplet state and thus a power law for the specific heat and a vanishing susceptibility for vanishing temperature.

The finite-temperature properties of the $S = 1/2$ hyperkagome-lattice Heisenberg antiferromagnet have also been considered [15–17,19]. For the gapless quantum spin liquid of Ref. [15], it was argued that $c(T) \propto T^2$ at low T (similarly to what is observed for $Na_4Ir_3O_8$ [10]) and that $\chi(T)$ is constant at low T (again in agreement with experimental data for $Na_4Ir_3O_8$ [10]). Application of the pseudofermion functional renormalization group [19] also shows that $\chi(T)$ exhibits no divergence down to zero temperature but only a very weak increase. In addition, high-temperature series expansions for c and χ were developed and compared with the experimental data for $Na_4Ir_3O_8$ [17].

On the experimental side, apart from the mentioned iridate compound $Na_4Ir_3O_8$ [10], there are other candidates for a solid-state realization of the hyperkagome-lattice Heisenberg anitiferromagnet; see, e.g., Refs. [20–22]. Note, however, that the $5d$-based transition-metal oxides, such as $Na_4Ir_3O_8$, are known for having a large spin-orbit coupling so that the pure nearest-neighbor Heisenberg Hamiltonian apparently should be augmented by other terms relevant for such materials [23]. Detailed comparisons of $c(T)$ and $\chi(T)$ between theory of Refs. [15,17,19] and experimental data for $Na_4Ir_3O_8$ [10] exhibit noticeable discreapancies roughly below $J/2$ (J is about

*Contact author: derzhko@icmp.lviv.ua

300 K for $Na_4Ir_3O_8$) and even at higher temperatures for the specific heat. The authors attributed this disagreement to an incomplete subtraction of nonmagnetic contributions to the experimentally measured $c(T)$ [17] and an insufficiency of the spin-isotropic Heisenberg model for description of the $S = 1/2$ hyperkagome antiferromagnet $Na_4Ir_3O_8$ [16,23]. Among various spin-anisotropic perturbations one may single out the Dzyaloshinskii-Moriya term, Kitaev term, and symmetric exchange anisotropic term [23].

The aim of the present paper is to examine the finite-temperature properties of the $S = 1/2$ hyperkagome-lattice Heisenberg antiferromagnet—a benchmark model of frustrated quantum magnets. At the moment, we do not intend to compare theoretical findings with experiments since there are no good solid-state examples of such a model yet. There are not so many methods applicable to tackle the thermodynamics of three-dimensional frustrated quantum spin systems. Quantum Monte Carlo suffers from the sign problem [24], exact diagonalization or finite-temperature Lanczos methods are restricted to too small lattices [25–27], the density-matrix renormalization group technique requires a mapping via a "snake" path to a one-dimensional system [28]. Besides, the pseudofermion functional renormalization group approach focuses on the wave-vector-dependent susceptibility [19], whereas one more universal method, the rotation-invariant Green's function method [29–35], has not been applied to the $S = 1/2$ hyperkagome-lattice Heisenberg antiferromagnet so far.

In our study, we utilize the high-temperature series expansions to the order of β^{16} ($\beta = 1/T$) provided by Singh and Oitmaa in Ref. [17]. Singh and Oitmaa used the high-temperature series to compute various thermodynamic properties down to a temperature [36] of about $T \approx 0.25$ [17]. However, this range can be extended down to zero temperature if one combines the series expansion with possible assumptions about the low-energy spectrum of the spin model within the framework of the "entropy method." The entropy-method interpolation of high-temperature series expansions was suggested by Bernu and Misguish [37] and later used in several studies [38–45]. In the present paper, we unite the series expansion [17] and the entropy method [37–39,41,42,44] to get the temperature dependence for the specific heat $c(T)$ and the uniform susceptibility $\chi(T)$ of the $S = 1/2$ hyperkagome-lattice Heisenberg antiferromagnet over the full temperature range. We also obtain a prediction for the ground-state energy of the model e_0, which provides self-consistency of the entropy-method calculations. Our entropy-method results are accompanied by finite-temperature Lanczos method data for finite lattices up to 36 sites.

The remainder of this paper is organized as follows. In Sec. II we introduce the model and briefly explain the methods to be used for obtaining the thermodynamic quantities. Then, in Sec. III, we report our results for the ground-state energy e_0, the specific heat $c(T)$, and the uniform susceptibility $\chi(T)$. Finally, we summarize our findings in Sec. IV.

II. MODEL AND METHODS

The hyperkagome lattice has been described in several papers. It can be viewed as a three-dimensional network of corner-sharing triangles with 12 sites in a cubic unit cell.

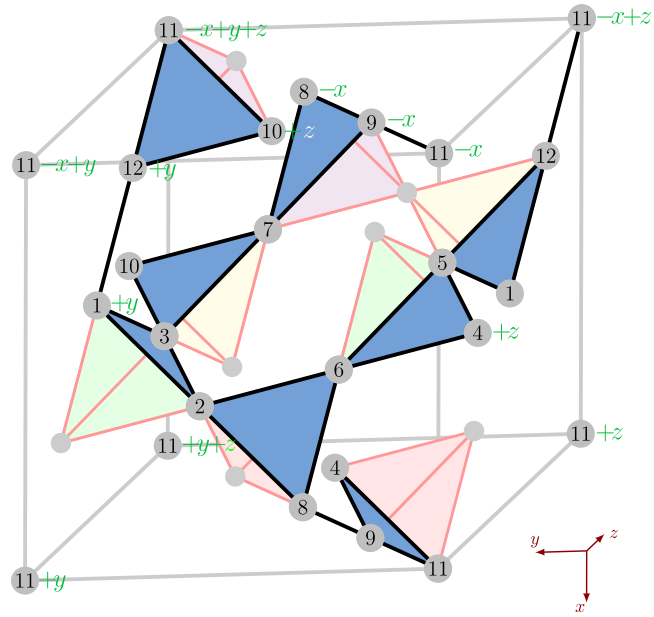

FIG. 1. The hyperkagome lattice. The unit cell contains 12 equivalent sites $\boldsymbol{r}_1, \ldots, \boldsymbol{r}_{12}$ (1) denoted as $1, \ldots, 12$. Each site is connected to its four closest neighbors by bonds (black lines). For more details of the lattice see the main text. We also display the underlying pyrochlore lattice.

It also can be viewed as a 1/4 depleted pyrochlore lattice, meaning that three out of the four sites in every tetrahedron are occupied by spins. As a result, each spin of the three-dimensional hyperkagome lattice has only four nearest neighbors just as for the two-dimensional kagome lattice. There are several different conventions regarding the coordinates of lattice sites (see, e.g., Refs. [23,46–48]). According to Fig. 1, we define the sites on the hyperkagome lattice by $\boldsymbol{R}_{\boldsymbol{n}\alpha} = \boldsymbol{R}_{\boldsymbol{n}} + \boldsymbol{r}_\alpha$. Here $\boldsymbol{R}_{\boldsymbol{n}} = n_x\boldsymbol{e}_x + n_y\boldsymbol{e}_y + n_z\boldsymbol{e}_z$, where n_x, n_y, n_z are integers and $\boldsymbol{e}_x = (1, 0, 0)$, $\boldsymbol{e}_y = (0, 1, 0)$, $\boldsymbol{e}_z = (0, 0, 1)$, generates a simple cubic lattice. Moreover, the origins of the 12 equivalent sites in the unit cell may be defined by $\boldsymbol{r}_\alpha$, $\alpha = 1, \ldots, 12$ with

$$\begin{aligned}
&\boldsymbol{r}_1 = \tfrac{1}{4}(-2, 0, 2), \quad \boldsymbol{r}_2 = \tfrac{1}{4}(-1, 3, 2), \quad \boldsymbol{r}_3 = \tfrac{1}{4}(-2, 3, 1),\\
&\boldsymbol{r}_4 = \tfrac{1}{4}(-1, 1, 0), \quad \boldsymbol{r}_5 = \tfrac{1}{4}(-2, 1, 3), \quad \boldsymbol{r}_6 = \tfrac{1}{4}(-1, 2, 3),\\
&\boldsymbol{r}_7 = \tfrac{1}{4}(-3, 2, 1), \quad \boldsymbol{r}_8 = \tfrac{1}{4}(0, 2, 2), \quad \boldsymbol{r}_9 = \tfrac{1}{4}(0, 1, 1),\\
&\boldsymbol{r}_{10} = \tfrac{1}{4}(-3, 3, 0), \quad \boldsymbol{r}_{11} = (0, 0, 0), \quad \boldsymbol{r}_{12} = \tfrac{1}{4}(-3, 0, 3).
\end{aligned} \tag{1}$$

In Fig. 1, we denote $\boldsymbol{r}_1, \ldots, \boldsymbol{r}_{12}$ by $1, \ldots, 12$. In addition, we display 13 sites of the nearby unit cells by $11 - x + y + z$, $11 - x + z$, $8 - x$, and so on, where, e.g., $11 - x + y + z$ means $\boldsymbol{r}_{11} - \boldsymbol{e}_x + \boldsymbol{e}_y + \boldsymbol{e}_z$, and so on.

In the present paper we consider the isotropic Heisenberg Hamiltonian on the hyperkagome lattice, which is given by

$$H = \sum_{\langle \boldsymbol{m}\alpha;\boldsymbol{n}\beta\rangle} \boldsymbol{S}_{\boldsymbol{m}\alpha} \cdot \boldsymbol{S}_{\boldsymbol{n}\beta}. \tag{2}$$

No extra interactions which may be relevant for solid-state compounds like $Na_4Ir_3O_8$ are included here, i.e., we treat a kind of idealized minimal model without complicated details but which already provides an interplay between geometrical

frustration and quantum and thermal fluctuations. In Eq. (2), the sum runs over the nearest-neighbor bonds of the hyperkagome lattice and $\boldsymbol{S}_{m\alpha}$ represents the $S = 1/2$ spin-vector operator at the lattice site $\boldsymbol{R}_{m\alpha}$. Expanding the sum in Eq. (2) for fixed $\boldsymbol{m}$, one gets 24 bonds, that is, 15 bonds connecting the sites within the unit cell with the same cell index $\boldsymbol{m}$ and 9 bonds connecting the sites of the unit cell $\boldsymbol{m}$ with the sites of the neighboring unit cells $\boldsymbol{m} - \boldsymbol{e}_x$, $\boldsymbol{m} - \boldsymbol{e}_y$, $\boldsymbol{m} - \boldsymbol{e}_z$, $\boldsymbol{m} - \boldsymbol{e}_x + \boldsymbol{e}_y$, $\boldsymbol{m} + \boldsymbol{e}_x - \boldsymbol{e}_z$, and $\boldsymbol{m} + \boldsymbol{e}_y - \boldsymbol{e}_z$; see Fig. 1. The remaining 4 bonds in Fig. 1, i.e., the ones which connect the sites $1 + y$ and $12 + y$, $8 - x$ and $9 - x$, $9 - x$ and $11 - x$, and $11 - x + y + z$ and $12 + y$ (cf. the bonds connecting the sites 1 and 12, 8 and 9, 9 and 11, and $11 - x + z$ and 12), are shown here for the sake of clarity.

It is worth noting that the hyperkagome lattice has similarities with the two-dimensional kagome lattice (corner-sharing triangles in two dimensions), as well as with the three-dimensional pyrochlore lattice (corner-sharing tetrahedrons in three dimensions), which could be considered the "mother" crystal structure; see Fig. 1. An important property is that all three lattices support dispersionless (flat) one-magnon bands. The shortest closed loop on the hyperkagome lattice beyond the triangles is a decagon; it involves 10 bonds. The shortest cycle on the kagome and pyrochlore lattices beyond the triangles is a hexagon; it involves six bonds. Since the even-numbered regular polygon (decagon or hexagon) is surrounded by isosceles triangles, the single-spin-flip state $\sum_{j\in\text{polygon}}(-1)^j S_j^-|\uparrow\ldots\uparrow\rangle$ cannot escape the polygon due to destructive quantum interference and one faces a localized-magnon state, which lives on the respective decagon or hexagon, and belongs to a flat band, for more details see Refs. [49,50].

In the remaining part of this section, we briefly explain the exploited methods: Numerics for finite-size lattices and high-temperature series complemented with the entropy-method interpolation. Here we only report the key elements necessary to state our results in Sec. III.

First, we determine numerically temperature dependencies for periodic lattices of $N = 12$ sites (exact diagonalization) and $N = 24$, 36 sites (finite-temperature Lanczos method); for a similar study of the $S = 1/2$ pyrochlore-lattice Heisenberg antiferromagnet see Refs. [42,51]. Since the unit cell for the hyperkagome lattice contains 12 sites, finite-lattice numerics is restricted to one unit cell [15] and two or three unit cells arranged as a chain. Within the finite-temperature Lanczos method, the sum over an orthonormal basis in the partition function is replaced in a Monte Carlo fashion by a much smaller sum over R random vectors where each random vector is employed for a trace estimation [25]. In the present study we take $R = 200$ for $N = 24$ and $R = 20$ for $N = 36$. More details about finite-lattice calculations can be found in Refs. [25–27,52,53]. Our numerical results for finite-size lattices are reported and discussed in Sec. III.

Second, we utilize the high-temperature series expansion up to 16th order, which was reported in Ref. [17] (the Magdeburg HTE code [54,55] yields the same series of the specific heat and the static uniform susceptibility, however, only up to 13th order), and employ the entropy method [37–39] to obtain temperature dependencies at all temperatures for infinite lattice.

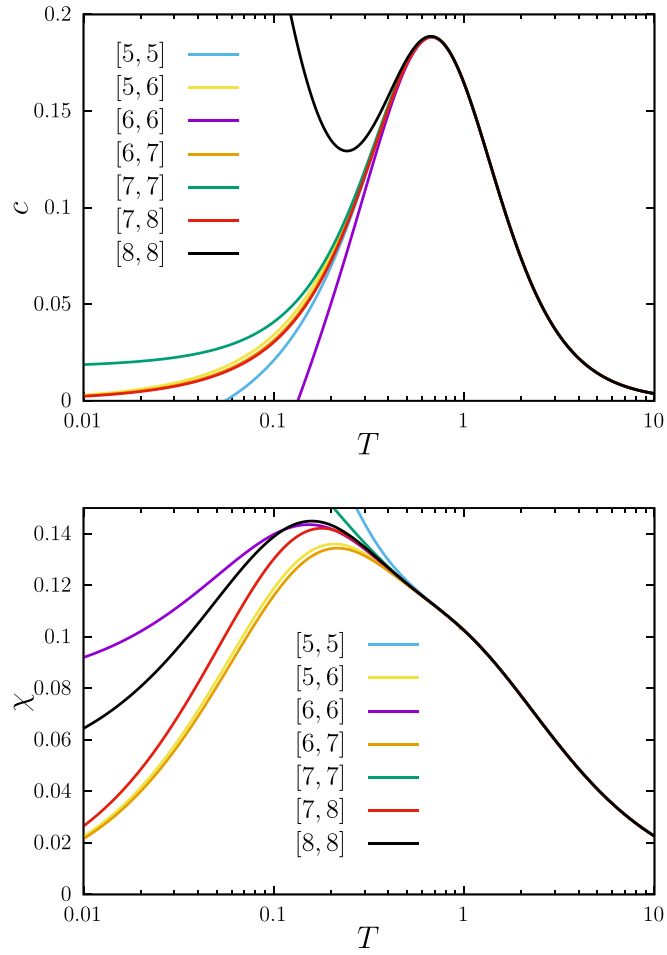

FIG. 2. Padé approximants of the high-temperature series [17] for (top) the specific heat and (bottom) the uniform susceptibility. They start to deviate from each other in both panels below $T \approx 0.5$.

As is well known, the raw high-temperature series expansion may be improved by simple Padé approximants $[u, d](T) = P_u(\beta)/Q_d(\beta)$. Here $P_u(\beta)$ and $Q_d(\beta)$ are polynomials of order u and d, $u + d \leqslant 16$, and the series expansion of $[u, d](T)$ coincides with the high-temperature series of c or χ up to 16th order with respect to $\beta = 1/T$. Comparing close to diagonal Padé approximants in Fig. 2, we conclude that they start to deviate notably one from another below $T \approx 0.5$ and thus can reproduce the high-temperature peak of $c(T)$ at $T \approx 0.67$, but not any of the specific features of $\chi(T)$ since $\chi(T)$ increases monotonously to temperatures well below $T = 0.5$ and also has got its maximum below $T = 0.5$.

Within the entropy method [37–39] one interpolates the entropy (per site) s as a function of the mean (internal) energy (per site) e, $s(e)$. As e approaches its maximal value $e_\infty = E(T \to \infty)/N = \text{tr}(H)/N = 0$, the entropy is known from high-temperature series expansion, $s(e) = \ln 2 + \sum_{i>1} a_i e^i$ (i.e., the coefficients $a_2, \ldots, a_{16}$ are known; see Ref. [37]). As e approaches its minimal (ground-state) value e_0, the entropy behaves as $s(e) \propto (e - e_0)^{\alpha/(1+\alpha)}$ if $c(T) = AT^\alpha$ for $T \to 0$ (gapless low-energy excitations) or as $s(e) \propto -[(e - e_0)/\Delta](\ln[\Delta(e - e_0)] - 1)$ if $c(T) \propto e^{-\Delta/T}/T^2$ for $T \to 0$ (gapped low-energy excitations). Next, we interpolate, instead

of $s(e)$, an auxiliary function $G(e)$, different for the two types of low-energy excitations (the choice of $G(e)$ was discussed in detail in Refs. [37,38]), which immediately gives $s(e)$. Such approximate quantities acquire the subscript "app." For the gapless case we have

$$G(e) = \frac{[s(e)]^{\frac{1+\alpha}{\alpha}}}{e-e_0} \to G_{\rm app}(e) = \frac{(\ln 2)^{\frac{\alpha}{1+\alpha}}}{-e_0}\frac{P_u(e)}{Q_d(e)};$$
$$s_{\rm app}(e) = [(e-e_0)G_{\rm app}(e)]^{\frac{\alpha}{1+\alpha}}. \quad (3)$$

And for the gapped case we have

$$G(e) = (e-e_0)\left[\frac{s(e)}{e-e_0}\right]' \to G_{\rm app}(e) = \frac{\ln 2}{e_0}\frac{P_u(e)}{Q_d(e)};$$
$$\frac{s_{\rm app}(e)}{e-e_0} = \frac{\ln 2}{-e_0} - \int_e^0 {\rm d}\xi \frac{G_{\rm app}(\xi)}{\xi - e_0}. \quad (4)$$

Here $P_u(e)$ and $Q_d(e)$ are the polynomials of order u and d, $u+d \leqslant 16$, and the series expansion of the quotient $[u,d](e) = P_u(e)/Q_d(e)$ coincides with the Maclaurin series of $G(e)$ known up to 16th order. Besides, the prime denotes the derivative with respect to e. Knowing the dependence $s(e)$, we obtain the desired temperature dependence of the specific heat $c(T)$ in parametric form: $T = 1/s'(e)$ and $c = -[s'(e)]^2/s''(e)$. Finally, we can calculate either the prefactor A, $A_{\rm app} = [\alpha^{1+\alpha}/(1+\alpha)^\alpha][G_{\rm app}(e_0)]^\alpha$, for the gapless case or the energy gap Δ, $\Delta_{\rm app} = -1/G_{\rm app}(e_0)$, for the gapped case. In the presence of a (small) external magnetic field h one gets the entropy $s_{\rm app}(e,h)$ which yields the uniform susceptibility χ via the relations: $m = [1/s'(e,h)]\partial s(e,h)/\partial h$, $\chi = m/h$ $(h \to 0)$. For further details see Refs. [37–39,41,42,44].

Thus, to obtain the thermodynamic quantities within the framework of the entropy method one needs, besides the high-temperature series for c and χ, to know (i) the ground-state energy e_0, (ii) how $c(T)$ vanishes as $T \to 0$, and (iii) the value of $\chi_0 \equiv \chi(T=0)$ in the case of gapless low-energy excitations. Even if the precise value of e_0 is not available and both gapless and gapped excitations are acceptable, one can proceed as in Ref. [41]. First, one has to assume some reasonable value e_0 in order to explore a certain region of e_0 systematically. Second, one has to assume the exponent α in the case of a gapless spectrum or one has to assume that the spectrum is gapped. Then, for the assumed e_0 and gapless/gapped energy spectrum one has to calculate within the entropy method the specific heat $c(T)$ using all n_P available Padé approximants $[u,d](e)$. There are $n+1$ Padé approximants based on the series up to nth order. We discard from the very beginning four Padé approximants $[n,0]$, $[n-1,1]$, $[1,n-1]$, $[0,n]$ so that $n_P = n-3$. Next, one has to examine the "closeness" of all n_P profiles $c(T)$. To this end, we inspect them thoroughly from some high temperature T_i down to $T_f < T_i$ with temperature steps ΔT. If the absolute value of the difference of a certain c from the arithmetic mean value for this bundle, $\bar{c}$, at a running temperature T $(T_f \leqslant T \leqslant T_i)$ is less than, e.g., 0.001, then this c belongs to the set of "coinciding" Padé approximants. Otherwise, this Padé approximant is discarded and not considered for lower temperatures. According to Refs. [41,44], a large number of coinciding curves $n_{\rm cP}$, or more precisely a large value of $p = n_{\rm cP}/n_P$, provides evidence that the assumptions made about e_0 and the low-energy excitations are self-consistent.

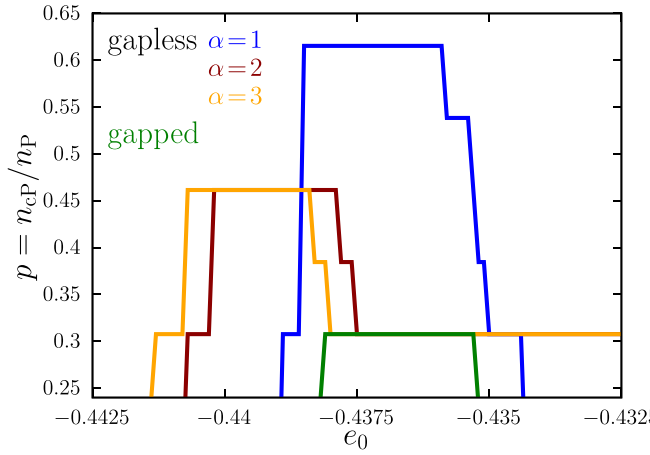

FIG. 3. The ratio of the number of "coinciding" entropy-method Padé approximants $n_{\rm cP}$ to the number of all considered entropy-method Padé approximants n_P, $p = n_{\rm cP}/n_P$, based on the series of 16th order as a function of the chosen value of e_0. Here $T_i = 0.5$, $\Delta T = 0.025$, $T_f = 0.1$; see the main text. We consider several assumptions, gapless and $\alpha = 1$ (blue), $\alpha = 2$ (red), $\alpha = 3$ (orange), or gapped (green) low-energy excitations.

In Fig. 3 we illustrate such an analysis based on $n_P = 13$ Padé approximants (obtained from the 16th order high-temperature series expansion) in Eqs. (3) or (4) for the specific heat $c(T)$ under the assumption of a gapless spectrum (blue, red, and orange) or a gapped spectrum (green). Here we set $T_i = 0.5$, $\Delta T = 0.025$, $T_f = 0.1$. If e_0 is taken in the range $[-0.438\,5, -0.435\,9]$ assuming a gapless spectrum and $\alpha = 1$, i.e., $c(T) = AT$ as $T \to 0$, then we find that $n_{\rm cP} = 8$ and $p \approx 0.62$. In addition, for the prefactor A we obtain the interval [5.62,7.74]. Similarly, if e_0 is taken in the range $[-0.440\,2, -0.437\,9]$ assuming $c(T) = AT^2$ as $T \to 0$, then we find that $n_{\rm cP} = 6$, $p \approx 0.46$, whereas A belongs to the interval [493,727]. And for e_0 taken in the range $[-0.440\,7, -0.438\,4]$ under the assumption $c(T) = AT^3$ as $T \to 0$, we find $n_{\rm cP} = 6$ and $p \approx 0.46$. Finally, assuming a gapped spectrum and taking e_0 in the range $[-0.438\,1, -0.435\,3]$, we find $p = 4/13 \approx 0.31$. In addition, the energy gap Δ for the lower $e_0 = -0.438\,1$ is 0.025, whereas for the higher $e_0 = -0.435\,3$ it is 0.018. In Fig. 3 we show the explicit dependence of p on e_0 under the mentioned assumptions on the behavior of $c(T)$ as $T \to 0$ to illustrate our reasonings.

Acting in accordance with the strategy of Refs. [41,44], we may estimate the entropy-method prediction for the ground-state energy e_0 as follows: Under the assumption of gapless excitations, e_0 depends on α but remains within the range $[-0.440\,7, -0.435\,9]$, whereas under the assumption of gapped excitations, $e_0 \in [-0.438\,1, -0.435\,3]$. In what follows, we use this missing input parameter e_0 for the entropy method, considering all assumptions about $c(T)$ as $T \to 0$, as well as the minimal and maximal values of e_0 to obtain the shaded areas for $c(T)$ and $\chi(T)$; see Sec. III B. We note in passing that the uniform susceptibility $\chi(T)$ is less convenient for seeking a large value of $p = n_{\rm cP}/n_P$, since it requires

the additional parameter χ_0 if the spectrum is gapless; see also Ref. [41].

More details about the entropy-method calculations can be found in Refs. [37–39,41,42,44]. Our entropy-method results are reported and discussed in Sec. III.

III. RESULTS

A. Ground-state energy e_0

We begin with the discussion of the ground-state energy of the $S = 1/2$ hyperkagome-lattice Heisenberg antiferromagnet. Various proposals about the nature of the ground state, i.e., spin liquids or valence-bond crystals, yield $e_0 = -0.424$ [15] or $e_0 = -0.430\,115$ [16]. Exact diagonalizations for $N = 12, 24, 36$ yield $-0.453\,74$, $-0.446\,33$, $-0.445\,10$, that, apparently, are underestimated values of the thermodynamically large systems. As explained above, to provide consistency of the entropy-method calculations, we have to assume for e_0 the values in the range $[-0.441, -0.435]$: This is a combination of several possible scenarios of either a gapless (with $\alpha = 1, 2, 3$) or a gapped energy spectrum. Yet another plausible simple approach to determine e_0 from the high-temperature series expansion, which uses monotonous decrease of $e(T)$ as T decreases to zero; see Ref. [6], Supplemental Material, Appendix D, yields e_0 about -0.448. The determination of e_0 based on the high-temperature series expansion seems to be rather formal, since it does not use any specific picture for the ground state of the model at hand. However, the experience from other models, including exactly solvable ones and precisely examined numerically ones, gives hints that it may yield quite reasonable predictions [41,44].

It is worth noting that the ground-state energy per site e_0 for the hyperkagome lattice is quite close to the one for the kagome lattice: $-0.438\,6(5)$ [56,57], $-0.438\,7$ [58], but is rather different from the one for the pyrochlore lattice: $-0.490(6)$ [6], $-0.483\,1(1)$ [7], -0.489 [9]. (Note that the interrelation is maintained for the energies per bond for the hyperkagome and kagome lattices, $e_0/2$, and the pyrochlore lattice, $e_0/3$.) This observation indicates that the hyperkagome and kagome systems share similar physics as $T \to 0$, which is different from the pyrochlore system.

B. Thermodynamic properties

We pass to the finite-temperature properties of the $S = 1/2$ hyperkagome-lattice Heisenberg antiferromagnet. First, in Fig. 4 we report the temperature dependence of the specific heat $c(T)$ and the uniform susceptibility $\chi(T)$ obtained for finite lattices of $N = 12,\ 24,\ 36$. Second, in Fig. 5 we report $c(T)$ and $\chi(T)$ obtained by the entropy method. Here several possibilities, i.e., the gapless spectrum with $\alpha = 1, 2, 3$ or the gapped spectrum, were considered; see blue, red, orange, or green curves, respectively. The ground-state energy e_0 was determined from the analysis of $c(T)$ as was explained in Sec. II. We used $[8, 8](e)$ in Eqs. (3) or (4) as well as the region of e_0 where p has a maximum; see Fig. 3, in order to estimate the spread of the derived functions. For the gapless excitations we set $\chi_0 = 0,\ 0.08,\ 0.12,\ 0.16$.

Let us now discuss the thermodynamic quantities of the $S = 1/2$ hyperkagome-lattice Heisenberg antiferromagnet in some detail. As it follows from the upper panel of Fig. 4, the high-temperature peak of the specific heat does not show any finite-size scaling; it is already provided by the calculations for one unit cell ($N = 12$). On these grounds, we thus conclude that the curve of the specific heat at temperatures of the high-temperature peak and above represents the thermodynamic limit [59]; see also $N = 36$ data in Fig. 5. The position of the low-temperature peak, on the other hand, does depend on the size. Moreover, the height decreases notably with growing N. The results of the entropy method in Fig. 5 refer to the infinite lattice. As it follows from the upper panel of Fig. 5, the specific heat $c(T)$ besides the high-temperature peak at $T \approx 0.67$ has an additional low-temperature maximum, which is about two times smaller and occurs below $T = 0.05$ under both assumptions of gapless and gapped excitations. For the case of the gapless excitations with $\alpha = 1$, the low-temperature peak is so small that it is perceived as a shoulder; see the blue curve in the upper panel of Fig. 5.

As can be seen in the lower panel of Fig. 4, the maximum of $\chi(T)$ has a mild dependence on system size: The peak position is about 0.204, 0.168, and 0.158 for $N = 12$, 24,

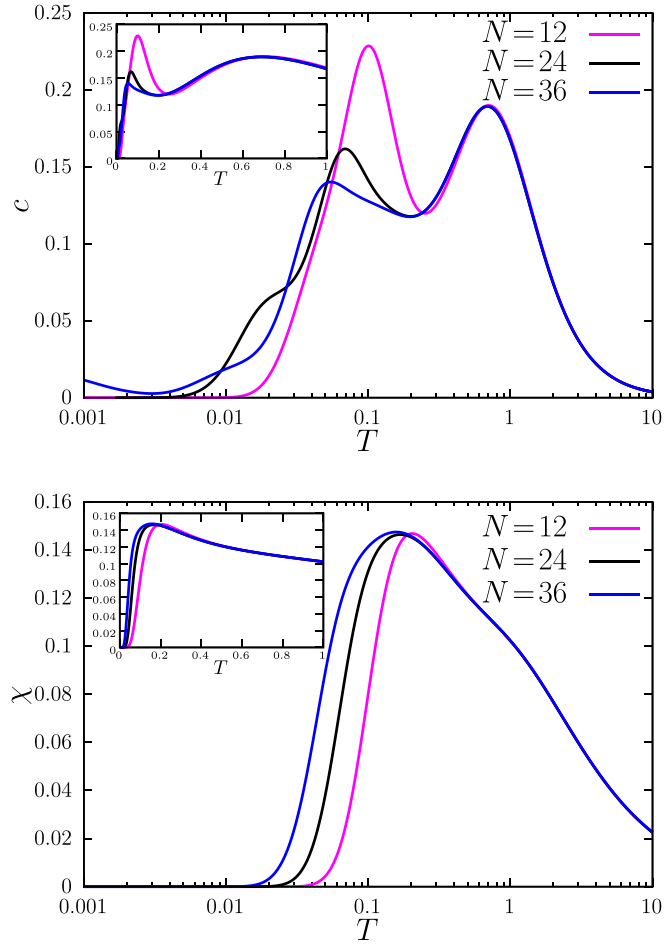

FIG. 4. Finite-lattice results for (top) the specific heat and (bottom) the uniform susceptibility of the $S = 1/2$ hyperkagome-lattice Heisenberg antiferromagnet (the insets present results in the linear temperature scale). Exact-diagonalization ($N = 12$) and finite-temperature Lanczos method ($N = 24$ and $N = 36$) data. The results for $N = 24$ and $N = 36$ differ from each other below about $T \approx 0.2$.

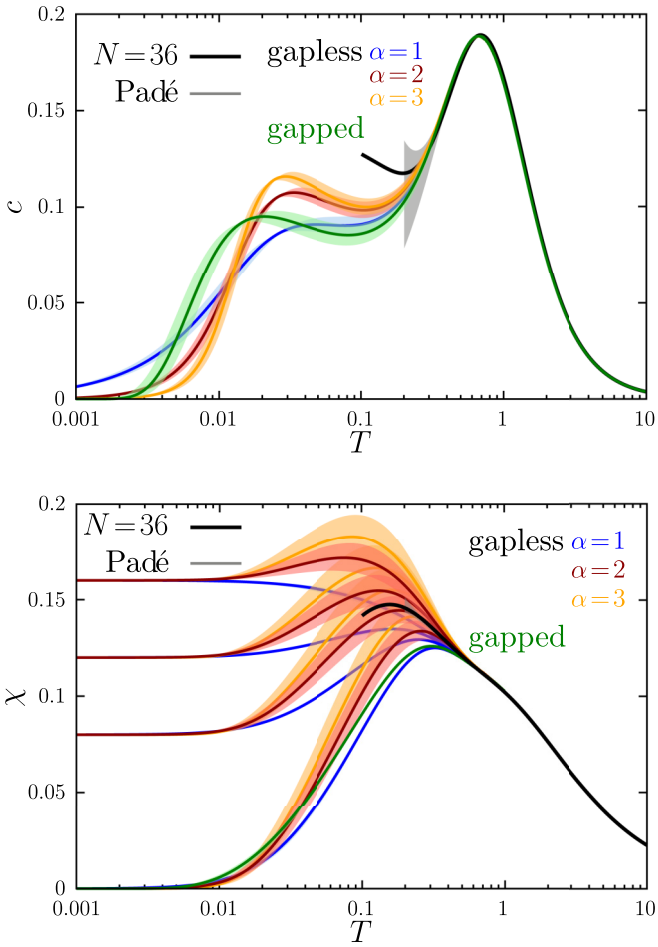

FIG. 5. Entropy-method results for (top) the specific heat and (bottom) the uniform susceptibility of the $S = 1/2$ hyperkagome-lattice Heisenberg antiferromagnet. Blue, red, and orange curves correspond to the gapless spectrum ($c = AT^{\alpha}$ as $T \to 0$) with $\alpha = 1, 2, 3$, respectively, and green ones to the gapped spectrum ($c \propto e^{-\Delta/T}/T^2$ as $T \to 0$). The shaded area (light blue, light red, light orange, and light green) represents the region of e_0 where p has a maximum (see Fig. 3). Note that the shaded areas around blue and green $\chi(T)$ curves are narrow and almost invisible. We also show $N = 36$ data (black, $T \geqslant 0.1$) and two simple Padé approximants [7,7] and [8,8] for $c(T)$ and $\chi(T)$ and color in gray the region between them ($T \geqslant 0.2$); the shaded region for $\chi(T)$ is rather narrow and can be seen only just above $T = 0.2$. In the case of gapless excitations, we examine the four values of χ_0: 0, 0.08, 0.12, and 0.16.

and 36, respectively. Moreover, the height remains practically unchanged being around 0.147 for all N. This behavior can be traced back to the size of the singlet-triplet gap for these systems. Its value is $\Delta_{s\text{-}t} \approx 0.383, 0.216, 0.136$ for $N = 12, 24, 36$, respectively. According to the entropy-method analysis reported in the lower panel of Fig. 5, the uniform susceptibility $\chi(T)$ behaves identically at T above about 0.5 for gapless and gapped excitations. For lower temperatures, the behavior of $\chi(T)$ depends on the adopted scenario and the χ_0 value for gapless excitations. In the case of gapless spin excitations, the uniform susceptibility approaches $\chi_0 > 0$ as $T \to 0$ and displays or does not display a maximum roughly below $T = 0.3$ depending on the specific value χ_0, cf. blue, red, orange curves in the lower panel of Fig. 5.

An important general message that can be taken from Fig. 5 is that the entropy-method and finite-system numerical data (and even simple Padé approximants for χ) favor the assumption of a gapless spectrum and a quadratically vanishing specific heat at low temperature with finite χ_0 around 0.1. However, a linear decay of the specific heat cannot be excluded.

It is worthy to put our results for the hyperkagome lattice in the context of prior work for the kagome and pyrochlore lattices. Concerning $c(T)$ (the upper panels of Figs. 4 and 5), its features at least at intermediate temperatures and above, are quite similar to what is known for the kagome-lattice and also the square-kagome-lattice case (a peak at $T = 0.67$, a shoulder of two times smaller height for $0.1 < T < 0.25$ [60,61]), but differ from those for the pyrochlore-lattice case, where only one peak in $c(T)$, but no additional low-temperature feature such as peak or shoulder was found [42,62]. Concerning $\chi(T)$ (the lower panels of Figs. 4 and 5), it resembles the maximum of $\chi(T)$ for the finite-size kagome lattices [60] and for the infinite kagome lattice analyzed by the entropy method [39]. In contrast, for the pyrochlore lattice we have several scenarios, none of which can be excluded to date [42,62,63]. Thus, we may conclude that the three-dimensional hyperkagome lattice is closer to highly frustrated two-dimensional lattices (kagome, square-kagome) than to the three-dimensional pyrochlore lattice. However, it is worth noting the difference: For the kagome lattice, the low-temperature specific heat $c(T)$ below the major peak moves collectively to higher temperatures with increasing N [60] resulting in a low-temperature shoulder of the main peak in the thermodynamic limit [64]. This is opposite to what is observed for the hyperkagome lattice (recall the top panel of Fig. 4). Here the specific heat assumes rather large values for temperatures below the major peak—larger than for the kagome system—which with increasing system size shrink and move towards lower temperatures.

IV. SUMMARY AND OUTLOOK

In the present paper, we used finite-lattice calculations and high-temperature series expansions up to 16th order [17] complemented by plausible assumptions about low-temperature properties according to the entropy method to obtain the specific heat $c(T)$ and the uniform susceptibility $\chi(T)$ of the $S = 1/2$ hyperkagome-lattice Heisenberg antiferromagnet at all temperatures. Finite-lattice calculations are suitable to discuss the thermodynamics above $T = 0.2$, cf. $N = 24$ and $N = 36$ data in Fig. 4. The entropy method requires the knowledge of ground state and low-energy excitations which is currently not available. Therefore, we tested several scenarios (gapless excitations with various exponents for a power-law decay of $c(T \to 0)$ and values of χ_0 or gapped excitations) and examined the coherence of the obtained results. Our main findings are as follows. We observe a low-temperature peak in $c(T)$ (almost a shoulder for $\alpha = 1$) at $T < 0.05$, i.e., well below the main high-temperature peak. $\chi(T)$ below $T = 0.5$ relies heavily on the adopted scenario. Combining finite-lattice and entropy-method results gives evidence in favor of gapless

spin excitations with a quadratic low-temperature specific heat decay (although a linear one cannot be ruled out) and finite χ at $T = 0$ around 0.1. Such results agree with the proposal of a gapless quantum spin liquid in Ref. [15] and the pseudofermion functional renormalization group study of Ref. [19]. As a by-product, we have extracted the ground-state energy e_0 with a procedure explained in Sec. II. Although the value of e_0 depends on the adopted scenario, it was always restricted to $[-0.441, -0.435]$. We have found that the thermodynamics of the three-dimensional hyperkagome-lattice Heisenberg antiferromagnet is quite similar to the two-dimensional kagome-lattice one, but differs from that on the pyrochlore lattice.

Future work on the thermodynamics of the $S = 1/2$ hyperkagome-lattice Heisenberg antiferromagnet may be related to application of specific tools to tackle the problem. For instance, this model represents a so-called flat-band system: The one-magnon energy spectrum has a fourfold degenerate dispersionless band, which is the lowest-energy band. The flat-band states will be relevant at high fields and low temperatures and their dominant contribution to thermodynamics can be elaborated by special methods of flat-band systems; see Refs. [49,50]. Such a program has been realized for the $S = 1/2$ kagome-lattice and pyrochlore-lattice Heisenberg antiferromagnets in Refs. [65,66], and it might be applicable here, too.

ACKNOWLEDGMENTS

T.H. was supported by the fellowship of the President of Ukraine for young scholars and by the Projects of research works of young scientists of the National Academy of Sciences of Ukraine (Project No. 29-04/18-2023, Frustrated quantum magnets at finite temperatures). O.D. thanks J. Strečka for the kind hospitality at the MECO48 conference. O.D. acknowledges the kind hospitality of the University of Bielefeld in October–December of 2023 (supported by Erasmus+ and DFG). This work was supported by the Deutsche Forschungsgemeinschaft (DFG SCHN 615/28-1 and RI 615/25-1). T.H., T.K., and O.D. acknowledge the support through the EURIZON project (Project No. 3025 "Frustrated quantum spin models to explain the properties of magnets over wide temperature range"), which is funded by the European Union under Grant No. 871072.

[1] Edited by C. Berthier, L. P. Lévy, and G. Martinez, *High Magnetic Fields: Applications in Condensed Matter Physics and Spectroscopy* (Springer, Berlin, 2002), Vol. 595.

[2] Edited by U. Schollwöck, J. Richter, D. J. J. Farnell, and R. F. Bishop, *Quantum Magnetism* (Springer, Berlin, 2004), Vol. 645.

[3] Edited by H. T. Diep, *Frustrated Spin Systems* (World Scientific, Singapore, 2005).

[4] C. Lacroix, P. Mendels, and F. Mila, *Introduction to Frustrated Magnetism—Materials, Experiments, Theory*, Springer Series in Solid-State Sciences (Springer, Berlin, 2011), Vol. 164.

[5] B. Canals and C. Lacroix, Pyrochlore antiferromagnet: A three-dimensional quantum spin liquid, Phys. Rev. Lett. **80**, 2933 (1998).

[6] I. Hagymási, R. Schäfer, R. Moessner, and D. J. Luitz, Possible inversion symmetry breaking in the $S = 1/2$ pyrochlore Heisenberg magnet, Phys. Rev. Lett. **126**, 117204 (2021).

[7] N. Astrakhantsev, T. Westerhout, A. Tiwari, K. Choo, A. Chen, M. H. Fischer, G. Carleo, and T. Neupert, Broken-symmetry ground states of the Heisenberg model on the pyrochlore lattice, Phys. Rev. X **11**, 041021 (2021).

[8] M. Hering, V. Noculak, F. Ferrari, Y. Iqbal, and J. Reuther, Dimerization tendencies of the pyrochlore Heisenberg antiferromagnet: A functional renormalization group perspective, Phys. Rev. B **105**, 054426 (2022).

[9] R. Schäfer, B. Placke, O. Benton, and R. Moessner, Abundance of hard-hexagon crystals in the quantum pyrochlore antiferromagnet, Phys. Rev. Lett. **131**, 096702 (2023).

[10] Y. Okamoto, M. Nohara, H. Aruga-Katori, and H. Takagi, Spin-liquid state in the $S = 1/2$ hyperkagome antiferromagnet $Na_4Ir_3O_8$, Phys. Rev. Lett. **99**, 137207 (2007).

[11] J. M. Hopkinson, S. V. Isakov, H.-Y. Kee, and Y. B. Kim, Classical antiferromagnet on a hyperkagome lattice, Phys. Rev. Lett. **99**, 037201 (2007).

[12] M. J. Lawler, H.-Y. Kee, Y. B. Kim, and A. Vishwanath, Topological spin liquid on the hyperkagome lattice of $Na_4Ir_3O_8$, Phys. Rev. Lett. **100**, 227201 (2008).

[13] M. E. Zhitomirsky, Octupolar ordering of classical kagome antiferromagnets in two and three dimensions, Phys. Rev. B **78**, 094423 (2008).

[14] Y. Zhou, P. A. Lee, T.-K. Ng, and F.-C. Zhang, $Na_4Ir_3O_8$ as a 3D spin liquid with fermionic spinons, Phys. Rev. Lett. **101**, 197201 (2008).

[15] M. J. Lawler, A. Paramekanti, Y. B. Kim, and L. Balents, Gapless spin liquids on the three-dimensional hyperkagome lattice of $Na_4Ir_3O_8$, Phys. Rev. Lett. **101**, 197202 (2008).

[16] E. J. Bergholtz, A. M. Läuchli, and R. Moessner, Symmetry breaking on the three-dimensional hyperkagome lattice of $Na_4Ir_3O_8$, Phys. Rev. Lett. **105**, 237202 (2010).

[17] R. R. P. Singh and J. Oitmaa, High-temperature series expansion study of the Heisenberg antiferromagnet on the hyperkagome lattice: Comparison with $Na_4Ir_3O_8$, Phys. Rev. B **85**, 104406 (2012).

[18] Y. Wan and Y. B. Kim, Phenomenological approach to a hyperkagome spin liquid: Emergent gauge fields and spinons, Phys. Rev. B **94**, 224401 (2016).

[19] F. L. Buessen and S. Trebst, Competing magnetic orders and spin liquids in two- and three-dimensional kagome systems: Pseudofermion functional renormalization group perspective, Phys. Rev. B **94**, 235138 (2016).

[20] B. Koteswararao, R. Kumar, P. Khuntia, S. Bhowal, S. K. Panda, M. R. Rahman, A. V. Mahajan, I. Dasgupta, M. Baenitz, K. H. Kim, and F. C. Chou, Magnetic properties and heat capacity of the three-dimensional frustrated $S = \frac{1}{2}$ antiferromagnet $PbCuTe_2O_6$, Phys. Rev. B **90**, 035141 (2014).

[21] S. Chillal, Y. Iqbal, H. O. Jeschke, J. A. Rodriguez-Rivera, R. Bewley, P. Manuel, D. Khalyavin, P. Steffens, R. Thomale, A. T. M. N. Islam, J. Reuther, and B. Lake, Evidence for a

three-dimensional quantum spin liquid in $PbCuTe_2O_6$, Nat. Commun. **11**, 2348 (2020).

[22] B. Sana, M. Barik, M. Pregelj, U. Jena, M. Baenitz, J. Sichelschmidt, K. Sethupathi, and P. Khuntia, Magnetic properties of a spin-orbit entangled $J_{\text{eff}} = \frac{1}{2}$ three-dimensional frustrated rare-earth hyperkagome material, Phys. Rev. B **108**, 134413 (2023).

[23] B. Huang, Y. B. Kim, and Y.-M. Lu, Interplay of nonsymmorphic symmetry and spin-orbit coupling in hyperkagome spin liquids: Applications to $Na_4Ir_3O_8$, Phys. Rev. B **95**, 054404 (2017).

[24] P. Henelius and A. W. Sandvik, Sign problem in Monte Carlo simulations of frustrated quantum spin systems, Phys. Rev. B **62**, 1102 (2000).

[25] J. Jaklič and P. Prelovšek, Lanczos method for the calculation of finite-temperature quantities in correlated systems, Phys. Rev. B **49**, 5065 (1994).

[26] R. Schnalle and J. Schnack, Calculating the energy spectra of magnetic molecules: application of real- and spin-space symmetries, Int. Rev. Phys. Chem. **29**, 403 (2010).

[27] J. Schnack, J. Richter, and R. Steinigeweg, Accuracy of the finite-temperature Lanczos method compared to simple typicality-based estimates, Phys. Rev. Res. **2**, 013186 (2020).

[28] J. Ummethum, J. Schnack, and A. Läuchli, Large-scale numerical investigations of the antiferromagnetic Heisenberg icosidodecahedron, J. Magn. Magn. Mater. **327**, 103 (2013).

[29] P. M. Richards, Spin-wave theory and static correlations in a one-dimensional Heisenberg antiferromagnet, Phys. Rev. Lett. **27**, 1800 (1971).

[30] J. Kondo and K. Yamaji, Green's-function formalism of the one-dimensional Heisenberg spin system, Prog. Theor. Phys. **47**, 807 (1972).

[31] H. Shimahara and S. Takada, Green's function theory of the two-dimensional Heisenberg model—Spin wave in short range order, J. Phys. Soc. Jpn. **60**, 2394 (1991).

[32] A. F. Barabanov and V. M. Beresovsky, On the theory of the two-dimensional Heisenberg antiferromagnet with frustration on a square lattice, J. Phys. Soc. Jpn. **63**, 3974 (1994).

[33] S. Winterfeldt and D. Ihle, Theory of antiferromagnetic short-range order in the two-dimensional Heisenberg model, Phys. Rev. B **56**, 5535 (1997).

[34] P. Müller, A. Zander, and J. Richter, Thermodynamics of the kagome-lattice Heisenberg antiferromagnet with arbitrary spin S, Phys. Rev. B **98**, 024414 (2018).

[35] P. Müller, A. Lohmann, J. Richter, and O. Derzhko, Thermodynamics of the pyrochlore-lattice quantum Heisenberg antiferromagnet, Phys. Rev. B **100**, 024424 (2019).

[36] Temperatures are given as multiples of the exchange interaction. $T = 0.25$ thus means $T/J = 0.25$. In our study we set the nearest-neighbor Heisenberg antiferromagnetic interaction $J = 1$.

[37] B. Bernu and G. Misguich, Specific heat and high-temperature series of lattice models: Interpolation scheme and examples on quantum spin systems in one and two dimensions, Phys. Rev. B **63**, 134409 (2001).

[38] G. Misguich and B. Bernu, Specific heat of the $S = \frac{1}{2}$ Heisenberg model on the kagome lattice: High-temperature series expansion analysis, Phys. Rev. B **71**, 014417 (2005).

[39] B. Bernu and C. Lhuillier, Spin susceptibility of quantum magnets from high to low temperatures, Phys. Rev. Lett. **114**, 057201 (2015).

[40] H.-J. Schmidt, A. Hauser, A. Lohmann, and J. Richter, Interpolation between low and high temperatures of the specific heat for spin systems, Phys. Rev. E **95**, 042110 (2017).

[41] B. Bernu, L. Pierre, K. Essafi, and L. Messio, Effect of perturbations on the kagome $S = \frac{1}{2}$ antiferromagnet at all temperatures, Phys. Rev. B **101**, 140403(R) (2020).

[42] O. Derzhko, T. Hutak, T. Krokhmalskii, J. Schnack, and J. Richter, Adapting Planck's route to investigate the thermodynamics of the spin-half pyrochlore Heisenberg antiferromagnet, Phys. Rev. B **101**, 174426 (2020).

[43] V. Grison, P. Viot, B. Bernu, and L. Messio, Emergent Potts order in the kagome $J_1 - J_3$ Heisenberg model, Phys. Rev. B **102**, 214424 (2020).

[44] M. G. Gonzalez, B. Bernu, L. Pierre, and L. Messio, Ground-state and thermodynamic properties of the spin-$\frac{1}{2}$ Heisenberg model on the anisotropic triangular lattice, SciPost Phys. **12**, 112 (2022).

[45] T. Hutak, T. Krokhmalskii, O. Derzhko, and J. Richter, Spin-half Heisenberg antiferromagnet on a symmetric sawtooth chain: Rotation-invariant Green's functions and high-temperature series, Eur. Phys. J. B **96**, 50 (2023).

[46] H.-K. Jin and Y. Zhou, Classical and quantum order in hyperkagome antiferromagnets, Phys. Rev. B **101**, 054408 (2020).

[47] L. E. Chern and Y. B. Kim, Theoretical study of quantum spin liquids in $s = \frac{1}{2}$ hyper-hyperkagome magnets: Classification, heat capacity, and dynamical spin structure factor, Phys. Rev. B **104**, 094413 (2021).

[48] R. Pohle and L. D. C. Jaubert, Curie-law crossover in spin liquids, Phys. Rev. B **108**, 024411 (2023).

[49] O. Derzhko, J. Richter, A. Honecker, and H.-J. Schmidt, Universal properties of highly frustrated quantum magnets in strong magnetic fields, Low Temp. Phys. **33**, 745 (2007).

[50] O. Derzhko, J. Richter, and M. Maksymenko, Strongly correlated flat-band systems: The route from Heisenberg spins to Hubbard electrons, Int. J. Mod. Phys. B **29**, 1530007 (2015).

[51] V. R. Chandra and J. Sahoo, Spin-$\frac{1}{2}$ Heisenberg antiferromagnet on the pyrochlore lattice: An exact diagonalization study, Phys. Rev. B **97**, 144407 (2018).

[52] J. Schulenburg, software *spinpack* 2.58, Magdeburg University (2019), https://www-e.uni-magdeburg.de/jschulen/spin/.

[53] J. Richter and J. Schulenburg, The spin-1/2 $J_1 - J_2$ Heisenberg antiferromagnet on the square lattice: Exact diagonalization for $N = 40$ spins, Eur. Phys. J. B **73**, 117 (2010).

[54] H.-J. Schmidt, A. Lohmann, and J. Richter, Eighth-order high-temperature expansion for general Heisenberg Hamiltonians, Phys. Rev. B **84**, 104443 (2011).

[55] A. Lohmann, H.-J. Schmidt, and J. Richter, Tenth-order high-temperature expansion for the susceptibility and the specific heat of spin-s Heisenberg models with arbitrary exchange patterns: Application to pyrochlore and kagome magnets, Phys. Rev. B **89**, 014415 (2014).

[56] S. Yan, D. A. Huse, and S. R. White, Spin-liquid ground state of the $s = 1/2$ kagome Heisenberg antiferromagnet, Science **332**, 1173 (2011).

[57] S. Depenbrock, I. P. McCulloch, and U. Schollwöck, Nature of the spin-liquid ground state of the $s = 1/2$ Heisenberg model on the kagome lattice, Phys. Rev. Lett. **109**, 067201 (2012).

[58] A. M. Läuchli, J. Sudan, and R. Moessner, $s = \frac{1}{2}$ kagome Heisenberg antiferromagnet revisited, Phys. Rev. B **100**, 155142 (2019).

[59] In contrast, the results for the $S = 1/2$ pyrochlore-lattice Heisenberg antiferromagnet of $N = 32$ sites [42] reflect the thermodynamic limit only for $T > 0.7$, well above the temperature of the high-temperature peak of $c(T)$. Therefore, the finite-lattice results for the hyperkagome case allow a reliable discussion of thermodynamic properties for much lower temperatures down to $T \approx 0.2$.

[60] J. Schnack, J. Schulenburg, and J. Richter, Magnetism of the $N = 42$ kagome lattice antiferromagnet, Phys. Rev. B **98**, 094423 (2018).

[61] J. Richter, O. Derzhko, and J. Schnack, Thermodynamics of the spin-half square kagome lattice antiferromagnet, Phys. Rev. B **105**, 144427 (2022).

[62] R. Schäfer, I. Hagymási, R. Moessner, and D. J. Luitz, Pyrochlore $S = \frac{1}{2}$ Heisenberg antiferromagnet at finite temperature, Phys. Rev. B **102**, 054408 (2020).

[63] Y. Huang, K. Chen, Y. Deng, N. Prokof'ev, and B. Svistunov, Spin-ice state of the quantum Heisenberg antiferromagnet on the pyrochlore lattice, Phys. Rev. Lett. **116**, 177203 (2016).

[64] X. Chen, S.-J. Ran, T. Liu, C. Peng, Y.-Z. Huang, and G. Su, Thermodynamics of spin-1/2 kagome Heisenberg antiferromagnet: Algebraic paramagnetic liquid and finite-temperature phase diagram, Sci. Bull. **63**, 1545 (2018).

[65] M. E. Zhitomirsky and H. Tsunetsugu, Exact low-temperature behavior of a kagomé antiferromagnet at high fields, Phys. Rev. B **70**, 100403(R) (2004).

[66] M. E. Zhitomirsky and H. Tsunetsugu, Lattice gas description of pyrochlore and checkerboard antiferromagnets in a strong magnetic field, Phys. Rev. B **75**, 224416 (2007).